

# Thickness–radius relationship and spring constants of cholesterol helical ribbons

Boris Khaykovich<sup>a,1</sup>, Natalia Kozlova<sup>b</sup>, Wonshik Choi<sup>c,d</sup>, Aleksey Lomakin<sup>b</sup>, Chintan Hossain<sup>e,2</sup>, Yongjin Sung<sup>c</sup>, Ramachandra R. Dasari<sup>c</sup>, Michael S. Feld<sup>c</sup>, and George B. Benedek<sup>b,e,f,1</sup>

<sup>a</sup>Nuclear Reactor Laboratory, <sup>b</sup>Materials Processing Center, <sup>c</sup>George R. Harrison Spectroscopy Laboratory, <sup>e</sup>Department of Physics, and <sup>f</sup>Center for Materials Science and Engineering, Massachusetts Institute of Technology, 77 Massachusetts Avenue, Cambridge, MA 02139; and <sup>d</sup>Department of Physics, Korea University, Seoul 136-701, Korea

Contributed by George B. Benedek, July 15, 2009 (sent for review June 1, 2009)

**Using quantitative phase microscopy, we have discovered a quadratic relationship between the radius  $R$  and the thickness  $t$  of helical ribbons that form spontaneously in multicomponent cholesterol–surfactant mixtures. These helical ribbons may serve as mesoscopic springs to measure or to exert forces on nanoscale biological objects. The spring constants of these helices depend on their submicroscopic thickness. The quadratic relationship ( $R \propto t^2$ ) between radius and thickness is a consequence of the crystal structure of the ribbons and enables a determination of the spring constant of any of our helices solely in terms of its observable geometrical dimensions.**

biological force spectroscopy | elasticity of thin films | phase-contrast microscopy in biophysics

The elastic properties of meso- and nanoscale thin elastic strips forming helical ribbons or tubules, have been the focus of active recent research in both biophysics and nanoscience communities (1–7). We have discovered that in a number of complex aqueous solutions containing a sterol (cholesterol in particular) and a mixture of surfactants, the sterol molecules may self-assemble into ribbons of helical shape (8). The geometry of the helical ribbons is characterized by the radius, width, thickness, contour length, and pitch angle, see figure 1*a* in ref. 9. Remarkably, the pitch angle is always either 11° or 54°, whereas axial length, width, and radius vary by two orders of magnitude in the range from 1 to ≈100 μm. These helical ribbons are fascinating objects for fundamental studies (2, 8–10). Furthermore, because low-pitch helical ribbons have spring constants in the range of 0.5 to 500 pN/μm (2), and the elongation of these springs from 1 μm up to 100 μm can easily be observed microscopically, it follows that they can be used as mesoscopic spring scales to measure forces between nanoscale biological objects in the range from 0.5 pN to 50 nN. For this and other applications, the ability to readily determine the spring constants of individual helices is of crucial importance. In this article, we establish the relationship between the spring constant of the low-pitch cholesterol helical ribbons and its readily observable dimensions: width, radius, and length.

Originally, it had been thought that cholesterol helical ribbons formed in surfactant mixtures had liquid crystalline structure and that their shape was governed by elastic properties of liquid crystalline layer (9, 11, 12). Recently, we have shown by X-ray diffraction that these helical ribbons are, in fact, single crystals with structure closely resembling that of cholesterol monohydrate (10). Having in mind the single-crystal nature of our ribbons, we have proposed that their helical shape is determined by a balance between two terms in the free energy of deformation of the cholesterol crystalline strip (2). The first term, the spontaneous bending energy, favors curling toward one of the two faces of the ribbon and is linear in curvature,  $-K_s/R$ . The second term is the elastic energy of bending a strip. This energy increases equally upon curling toward either face of the ribbon, and it is proportional to the square of curvature,  $K_{el}/R^2$ . Mini-

mization of the sum of the two terms determines the radius of the helix,  $R = 2K_{el}/K_s$ . The quantitative theory for the observed geometrical and elastic properties of these helical ribbons is elaborated in ref. 2. If the ribbon is anisotropic,  $K_{el}(\psi)$  depends on the angle  $\psi$  between the axis of bending and the ribbon edge [note that in thin ribbons, only cylindrical deformations are possible (13)]. The equilibrium pitch angle  $\psi_0$  is the preferential bending direction, for which  $K_{el}(\psi)$  is minimal. When the crystalline helical ribbon with contour length  $s$  is stretched or compressed, its axial length  $l = s \sin \psi$ , and therefore its pitch angle changes. The ribbon is forced to bend in a less preferable direction than in equilibrium, and its elastic energy increases. That leads to axial rigidity and a corresponding spring constant. We have shown (2) that the spring constant  $K_{spring}$  of such a crystalline helical ribbon is determined by its width ( $w$ ), its contour length ( $s$ ), and its radius ( $R$ ) according to:

$$K_{spring} = \frac{8w}{R^2s} K_{\alpha}, \quad [1]$$

where the effective bending modulus

$$K_{\alpha} = \partial^2 K_{el}(\psi) / \partial (\sin \psi)^2 |_{\psi=\psi_0}$$

According to beam-bending theory for solid ribbons (13), we expect  $K_{\alpha}$  to be proportional to the cube of the thickness  $t$  of the strip,  $K_{\alpha} \propto t^3$ .

In this article, we report measurements of the thickness of cholesterol helical ribbons using quantitative phase microscopy (14, 15). We found a universal relationship, independent of solution conditions, between the thickness of the helix and its radius, consistent with  $R \propto t^2$ , as shown on Fig. 1. Because the bending modulus  $K_{\alpha}$  is determined only by internal elastic properties of the crystalline ribbon and its thickness, the radius of the helix can be used as a measure of the effective elastic modulus of the ribbon, according to relationship  $K_{\alpha} \propto t^3 \propto R^{3/2}$  with a universal proportionality coefficient. This relationship is of great importance for application purposes because it enables selection of cholesterol ribbons with desired spring constants based solely on microscopically observed geometrical parameters of the ribbon. Furthermore, we argue that our approach has broader applicability to a variety of nanoscale tubules and helical ribbons constituted of inorganic thin films (4, 5, 16) or thin single crystals such as ZnO and InP (17, 18).

Author contributions: B.K., W.C., A.L., R.R.D., M.S.F., and G.B.B. designed research; B.K., N.K., W.C., C.H., and Y.S. performed research; B.K., N.K., and W.C. analyzed data; and B.K., N.K., W.C., A.L., M.S.F., and G.B.B. wrote the paper.

The authors declare no conflict of interest.

<sup>1</sup>To whom correspondence may be addressed. E-mail: bkh@mit.edu or benedek@mit.edu.

<sup>2</sup>Present address: Department of Physics, Princeton University, Princeton, NJ 08544.

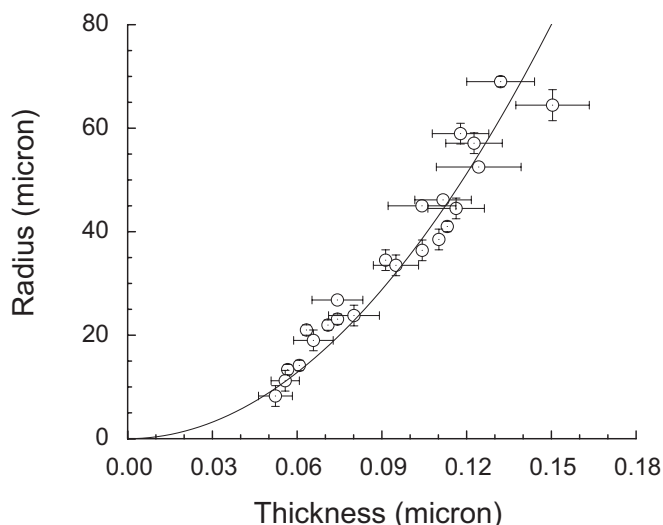


**Fig. 1.** Radius,  $R$ , vs. thickness,  $t$ , of cholesterol helical ribbons. The data are fitted to  $R = ct^2$ ,  $c = (3.56 \pm 0.11) \times 10^3 \mu\text{m}^{-1}$ . The radius is determined by direct observations using a standard bright-field microscope. The thickness was measured by using quantitative phase microscopy. Horizontal error bars were calculated from the errors in fitted positions of the peaks on Fig. 2B.

### Results

The thickness of the ribbons is  $< 200$  nm, which is below the diffraction-limited axial resolution of optical microscopes. To measure the thickness, we used quantitative phase microscopy (14, 15), which is developed for imaging of thin, nearly transparent biological specimens and allows examination of unperturbed individual ribbons in their solution environment. Although transparent, biological samples induce phase shifts in transmitted light. The phase shift,  $\Delta\phi$ , due to light passing through an object of thickness  $t$  rather than through the surrounding medium is  $\Delta\phi = 2\pi/\lambda_0 \Delta n t$ , where  $\Delta n$  is the difference in refractive indices between the object and the surrounding medium. Therefore, the thickness of the object can be calculated by using the following relation:

$$t = \frac{\Delta\phi \lambda_0}{2\pi \Delta n}. \quad [2]$$

To measure the phase shifts, we used a Mach-Zehnder interferometer integrated with an inverted microscope. The incident laser beam ( $\lambda_0 = 632.8$  nm) is split into two beams, one passing through the sample, and the other serving as a reference beam. When these two beams are recombined, an interference pattern is produced. This pattern reflects the phase shifts due to the optical path difference between the sample beam and the reference beam.

In Fig. 2A, we show a typical two-dimensional map of the phase distribution at the detector. The ribbon rests horizontally on a glass slide inside a fluid cell filled with the solution. Only the small part of the ribbon near the bottom is in focus and therefore seen on the picture. The pixels on Fig. 2A are color-coded corresponding to the value of phase difference between the sample and the reference beams. Statistical analysis of this phase image is shown on Fig. 2B. The histogram of the phase values at each pixel has two well-defined peaks. These two peaks correspond to the phase accumulated by the light beam propagating through the solution, or through the ribbon. Knowing this phase difference and the difference in refractive indices between the ribbons and the solvent, the thickness can be determined by using Eq. 2.

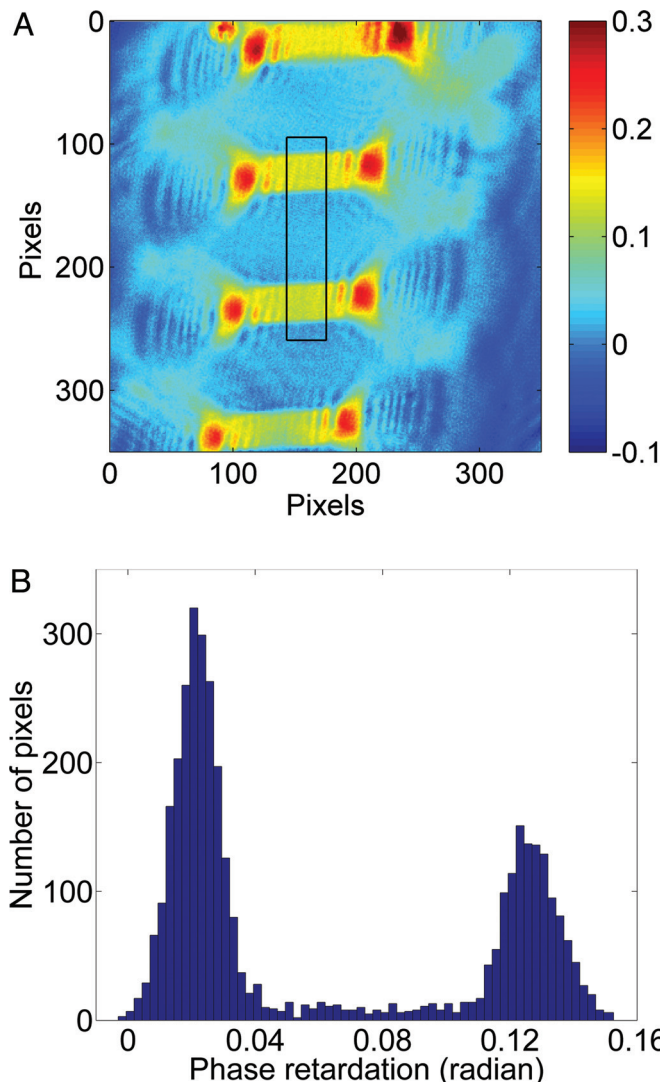


**Fig. 2.** Phase-contrast microscopy of cholesterol helical ribbons. (A) A color-coded phase image of a 68-nm-thick helical ribbon (100 pixels =  $15.3 \mu\text{m}$ ). The scale strip on the right shows the phase retardation in radians. Shown is the lower part of the helical ribbon, which is in focus of the phase microscope. (B) The histogram of phase retardations for pixels within the black rectangle on A. The peaks are fitted with a Gaussian distribution. The phase difference between the fitted centers of the two peaks is used in Eq. 2 to calculate the thickness of the ribbon.

To determine the thickness–radius relationship, we measured the thicknesses of a large number of helical ribbons of different radii. We used solutions of slightly different refractive indices produced by a variety of surfactant concentrations. The data are shown in Fig. 1. Because the rigidity vanishes at zero thickness, we expect that  $R(0) = 0$ ; hence, the data are consistent with the functional form:  $R = ct^2$ . The best fit for the parameter  $c$  gives:  $c = (3.56 \pm 0.11) 10^3 \mu\text{m}^{-1}$ .

### Discussion

From the practical point of view, we have demonstrated that it is possible to know the spring constant of any of our cholesterol helical ribbons simply from the easily measurable external dimensions of the ribbons. Indeed, substituting  $K_\alpha \propto t^3 \propto R^{3/2}$  into Eq. 1 we arrive at the relationship:

$$K_{\text{spring}} = \kappa \frac{w}{R^{1/2} s}, \quad [3]$$

with  $\kappa$  being a constant that depends only on elastic properties of the material constituting the ribbon. To take advantage of the Eq. 3,  $\kappa$  must be measured experimentally by measuring the spring constant for several ribbons. Here, we have used a previously measured value of  $K_{\text{spring}}$  for a single ribbon to give a preliminary estimate of  $\kappa$ . From ref. 2, the radius of that ribbon is  $R = (19.2 \pm 1) \mu\text{m}$ , therefore, the thickness is  $t = (0.073 \pm 0.003) \mu\text{m}$ ; the other dimensions are  $s = (803 \pm 30) \mu\text{m}$ ,  $w = (12.3 \pm 0.5) \mu\text{m}$ . The spring constant of this ribbon was  $K_{\text{spring}} = (4.8 \pm 0.9) \times 10^{-6} \text{ N/m}$  and, therefore, from Eq. 3:  $K_{\text{spring}} \cong 1.37 \times 10^{-6} w / (R^{1/2} s)$ .

The practical objective of our work is to make use of cholesterol helical ribbons with the pitch angle of  $11^\circ$  as a mechanical device. One such use is to measure the forces between nanoscopic objects by simply observing the extension of a helix tethered to them. The helices which self-assemble in multicomponent solutions containing sterols and appropriate surfactants are widely polydisperse in length, width, and radius. We have now shown that the radius of any given helix can serve as a measure of its thickness. This, in turn, enables us, by using Eq. 3, to know the spring constant of all observed springs and to select from the solution a helix most suited for the application in mind. To use these ribbons as force transducers, we are developing methods to tether to the helices by chemical activation of their surfaces. Tethering using an epoxy glue has been demonstrated already (2).

From the theoretical point of view, the bending deformation of a ribbon is characterized by its curvature  $1/R$ . When  $R$  is large, we can interpret the spontaneous bending energy ( $-K_s/R$ ) and the elastic energy ( $K_{\text{el}}/R^2$ ) as the first two terms in a Taylor expansion of the deformation free energy of the ribbon:

$$F - F_0 = -\frac{K_s}{R} + \frac{K_{\text{el}}}{R^2} + \dots \quad [4]$$

Minimizing the free energy with respect to  $R$ , we find that

$$R = \frac{2K_{\text{el}}}{K_s} \quad [5]$$

Physically, the first term in Eq. 4 might arise from a difference in surface tension between the two sides of the helical strip. Indeed, if  $S$  is the area of the middle plane of the strip, then the outer surface area is  $S(1 + t/(2R))$ , whereas the inner surface area is  $S(1 - t/(2R))$ . If  $\sigma_i$  is the surface tension of the inner side, and  $\sigma_o < \sigma_i$  is that of the outer, then the total surface free energy is  $S(\sigma_i + \sigma_o) - S(\sigma_i - \sigma_o)t/(2R)$ . Thus, if there is a surface tension difference between the inner and outer sides this will result in a linear in  $1/R$  contribution to the free energy, with  $K_s = St(\sigma_i - \sigma_o)/2$ . Experimentally, however, the relationship between thickness and the radius of the helix is not affected by the type and concentrations of surfactants added. Thus, the difference in surface tensions is a less than satisfying interpretation for the cause of spontaneous bending. Alternatively, the first term in Eq. 4 can arise from the spontaneous curling of all molecular layers in a ribbon because of the chiral nature of the sterol molecules. The  $K_s/R$  term in Eq. 4 is then proportional to ribbon volume,  $V = St$ , i.e., is linear in  $t$ . We stress that regardless of whether the spontaneous bending is caused by surface or bulk effects, the associated spontaneous bending term in the free energy is proportional to ribbon thickness.

Our experiments have shown that  $R \propto t^2$ . Because  $K_s \propto t$ , it follows from Eq. 5 that  $K_{\text{el}} \propto t^3$ , and the second term in the Taylor expansion (4) has the structure of the regular elastic energy of a solid body:  $V \cdot K t^2 / R^2$ , which is proportional to the second power of deformation  $t/R$ , elastic modulus  $K$ , and volume  $V$ . [For an isotropic solid ribbon,  $K = E/(24(1 - \sigma^2))$ , where  $E$  and  $\sigma$  are Young's modulus and Poisson's coefficient, respectively (13).]

This form of elastic free energy is consistent with and reconfirms our model of cholesterol helical ribbons as solid, crystalline objects, whose helical form is determined by relatively weak spontaneous bending forces arising from chirality of cholesterol molecules balanced by equally weak bending elasticity of a very thin solid band. If one includes the anisotropy of the elastic modulus  $K$ , the pitch angle and the longitudinal spring constant can be naturally explained, and analytically expressed (2, 19). On the other hand, the dependence of the elastic deformation energy on the third power of thickness is inconsistent with liquid-crystalline models for helical ribbons (9, 11, 12). Indeed, in those liquid-crystalline models, the molecular layers in the strip are not in register relative to one another. The deformation (e.g., the variation in the director orientation) of all layers is identical, the elastic energy of each layer is the same, and the total energy is proportional to the volume, giving a linear dependence on the thickness.

The growth of cholesterol crystals in a ribbon-like shape is a consequence of large differences in the rates of crystallization along different crystallographic axes. However, we observed no fixed relationship between length, width, and thickness of the ribbon. This is because crystallization at the ends, edges, and surface of the ribbon can be arrested in different ways by impurities or imperfections. As a result, our ribbons exist in a broad range of thickness, length, and width. In our work, we measured thickness ranging from  $0.06 \mu\text{m}$  to  $0.18 \mu\text{m}$ . On the other hand, ribbons just several bilayers, each of which is  $3.5 \text{ nm}$  thick, were observed by electron microscopy (20).

We wish to draw attention to another type of mesoscopic helical ribbons: thin film strips of Si, Si/SiGe, or InGaAs/GaAs grown on single-crystal substrates. Lattice constant mismatch between a film and a substrate creates elastic strain, leading to the curling of the strip into a helical ribbon (6, 21). These semiconductor helices, of  $1 \mu\text{m}$  in diameter and of tens of nanometers in thickness, are smaller than typical cholesterol ribbons. The spring constants of the Si/SiGe helical ribbons are several picoNewtons/micron (5). Similarly to cholesterol helical ribbons, the pitch angle of these ribbons is defined by the strip orientation of the substrate, and the anisotropy of the elastic constants of the bilayer (4, 5, 22). In contrast to our helical ribbons, the pitch angle can be varied in the manufacturing process. The radius vs. thickness of semiconductor helices and tubes is a matter of current debates (23). We believe that the analysis presented here and in ref. 2 may apply to elastic properties of these recently developed inorganic helical ribbons.

In conclusion, we have presented experiments and theoretical analysis, which confirms the validity of the crystal model for our cholesterol helical ribbons. Within the framework of this model, we have obtained an explicit formula for the spring constant of any chosen ribbon as a function of its readily observable external dimensions: length, width, and radius. In this way, we can now select, from a polydisperse solution, a ribbon with spring constant and size desired for a particular application. This is an important advance toward the practical utilization of these mesoscopic springs as devices for measuring and transducing forces between biological objects.

### Materials and Methods

We measured low-pitch helical ribbons (pitch angle of  $11^\circ$ ) formed in commercially available Chemically Defined Lipid Concentrate (CDLC), purchased from GIBCO. CDLC is a water solution that contains nonionic surfactants (Pluronic F-68 and Tween 80), a mixture of fatty acids and cholesterol. The molar ratio (percentage) of these components is 94.2:1.9:3.9. CDLC produces, with high yield, helical ribbons that remain stable for weeks. The helices in CDLC have radii ranging from  $5$  to  $100 \mu\text{m}$ , contour lengths between  $150$  and  $1,500 \mu\text{m}$ , and widths between  $1$  and  $20 \mu\text{m}$ .

The two-dimensional optical thickness of the sample, or a phase image, is reconstructed from the interference patterns. The phase difference between the sample and reference beams is measured by using a heterodyne technique

that utilizes acoustooptical modulators to shift the frequency of the reference beam by 1.25 kHz relative to that of the sample beam. Four interference images are taken by a camera with the frame rate of 5 kHz, four times larger than the frequency shift of reference beam. As a result, the relative phase between the sample and reference beams differs by  $\pi/2$  between consecutive interference images. The phase image of a sample is then calculated from these four interference images by using so-called phase-shifting interferometry algorithm (14). We measure the phase difference between the sample and reference beams with milliradian precision, which translates into a few nanometers resolution in the optical thickness of our samples.

Our instrument uses a coherent light source, and the phase images display a fixed pattern of diffraction from particles in the beam path, such as dust or micelles, as well as from the specimen itself. To remove the background diffraction pattern and thus enhance the signal-to-noise ratio of phase detection, we synthesize phase images taken at different angles of illumination, so that only images from the specimen in the focal plane add up constructively (15).

To use Eq. 2, we assume that our helices have the same index of refraction as cholesterol monohydrate crystals, which have essentially the same structure

as our helical strips (10). Because, to the best of our knowledge, this index of refraction has not been reported, we grew flat single crystals of cholesterol monohydrate, sufficiently thick to allow direct determination of their thickness microscopically by focusing on polystyrene beads adsorbed on the upper and lower surfaces and thin enough to permit the use of phase microscopy to measure phase retardation (in water solutions of potassium thiocyanate, having refractive indices of either  $n = 1.4152$  or  $1.4406$ ). Using Eq. 2, we found that the refractive index of cholesterol monohydrate along the  $c$  axis, which is perpendicular to both the plate shaped crystal and the ribbon surface, is  $n = 1.522 \pm 0.003$ . Interestingly, this value falls into the range  $1.49 \pm 0.06$ , which was measured by ellipsometry for a cholesterol monolayer on air–water interface (24).

**ACKNOWLEDGMENTS.** We gratefully acknowledge the support provided by the Department of Energy, Division of Materials Sciences and Engineering, Office of Basic Energy Sciences under Award DE-FG02-04ER46149. This work was also supported by National Center for Research Resources of the National Institutes of Health Grant P41-RR02594-18, National Science Foundation Grant DBI-0754339, and the Hamamatsu Corporation.

1. Schnur JM (1993) Lipid tubules—A paradigm for molecularly engineered structures. *Science* 262:1669–1676.
2. Smith B, Zastavker YV, Benedek GB (2001) Tension-induced straightening transition of self-assembled helical ribbons. *Phys Rev Lett* 87:278101.
3. Kessler DA, Rabin Y (2003) Stretching instability of helical springs. *Phys Rev Lett* 90:024301.
4. Bell DJ, et al. (2006) Fabrication and characterization of three-dimensional InGaAs/GaAs nanosprings. *Nano Lett* 6:725–729.
5. Grützmacher D, et al. (2008) Ultra flexible SiGe/Si/Cr nanosprings. *Microelectron J* 39:478–481.
6. Huang M, et al. (2005) Nanomechanical architecture of strained bilayer thin films: From design principles to experimental fabrication. *Adv Mater* 17:2860.
7. Starostin EL, van der Heijden GHM (2008) Tension-induced multistability in inextensible helical ribbons. *Phys Rev Lett* 101:084301.
8. Zastavker YV, et al. (1999) Self-assembly of helical ribbons. *Proc Natl Acad Sci USA* 96:7883–7887.
9. Chung DS, Benedek GB, Konikoff FM, Donovan JM (1993) Elastic free energy of anisotropic helical ribbons as metastable intermediates in the crystallization of cholesterol. *Proc Natl Acad Sci USA* 90:11341–11345.
10. Khaykovich B, et al. (2007) Structure of cholesterol helical ribbons and self-assembling biological springs. *Proc Natl Acad Sci USA* 104:9656–9660.
11. de Gennes PG (1987) Electrostatic buckling of chiral lipid bilayers. *C R Acad Sci Paris* 304:259–263.
12. Selinger JV, Spector MS, Schnur JM (2001) Theory of self-assembled tubules and helical ribbons. *J Phys Chem B* 105:7157–7169.
13. Landau LD, Lifshitz EM (1986) *Theory of Elasticity* (Pergamon, New York).
14. Fang-Yen C, et al. (2007) Imaging voltage-dependent cell motions with heterodyne Mach–Zehnder phase microscopy. *Opt Lett* 32:1572–1574.
15. Choi W, et al. (2007) Tomographic phase microscopy. *Nat Methods* 4:717–719.
16. Songmuang R, Deneke C, Schmidt O (2006) Rolled-up micro- and nanotubes from single-material thin films. *Appl Phys Lett* 89:223109.
17. Gao PX, et al. (2005) Conversion of zinc oxide nanobelts into superlattice-structured nanohelices. *Science* 309:1700–1704.
18. Shen GZ, et al. (2006) Single-crystalline cubic structured InP nanosprings. *Appl Phys Lett* 88:243106.
19. Smith B (2003) Geometric and elastic properties and mechanical phase separation phenomena in self-assembling mesoscopic helical springs. PhD Thesis (Massachusetts Institute of Technology, Cambridge, MA).
20. Weihs D, et al. (2005) Biliary cholesterol crystallization characterized by single-crystal cryogenic electron diffraction. *J Lipid Res* 46:942–948.
21. Prinz VY, et al. (2000) Free-standing and overgrown InGaAs/GaAs nanotubes, nanohelices and their arrays. *Physica E* 6:828–831.
22. Zhang L, et al. (2006) Anomalous coiling of SiGe/Si and SiGe/Si/Cr helical nanobelts. *Nano Lett* 6:1311–1317.
23. Zang J, Liu F (2008) Modified Timoshenko formula for bending of ultrathin strained bilayer films. *Appl Phys Lett* 92:021905.
24. Lafont S, et al. (1998) Monitoring the nucleation of crystalline films of cholesterol on water and in the presence of phospholipid. *J Phys Chem* 102:761–765.